EJTAS
ISSN 2786-7447
EUROPEAN JOURNAL OF THEORETICAL AND APPLIED SCIENCES
OPEN ACCESS
PEER REVIEWED

Theoretical Investigation on Monomer and Dimers of Inhibitor of Cytochrome P450 Enzymes: 1-Aminobenzotriazole

María E. Manzur, Pablo G. Cataldo, Maximiliano A. Iramain, María V. Castillo, Silvia Antonia Brandán *
Cátedra de Química General, Instituto de Química Inorgánica, Facultad de Bioquímica. Química y Farmacia, Universidad Nacional de Tucumán, Tucumán, Argentina

Article Information
Suggested Citation:
Manzur, M.E., Cataldo, P.G., Iramain, M.A., Castillo, M.V. & Brandán, S.A. (2023). Theoretical investigation on monomer and dimers of inhibitor of cytochrome P450 enzymes: 1-Aminobenzotriazole. *European Journal of Theoretical and Applied Sciences, 1*(3), 456-484.
DOI: 10.59324/ejtas.2023.1(3).45

*** Corresponding author:**
Silvia Antonia Brandán
e-mail:
silvia.brandan@fbqf.unt.edu.ar

Abstract:

In this research, structures and properties of monomer and two dimers (1 and 2) of inhibitor of cytochrome P450 enzymes, 1-Aminobenzotriazole (ABT) have been studied by using functional hybrid B3LYP/6-311++G** calculations. The very good correlations observed between theoretical and experimental ^{1}H-, ^{13}C-NMR, FT-IR and FT-Raman spectra suggest that C-H···N interactions of dimeric species should be expected in the solid phase, as was observed in the experimental crystalline structure of a quinolin benzotriazole derivative. NBO and AIM calculations suggest that dimer 2 with inverted positions of its monomers could be present in the solid phase because it evidence higher stabilities in both media. On the other hand, frontier orbitals studies support a higher reactivity of dimer 2 of ABT higher than the monomer and dimer 1, for which, the presence of dimer 2 containing N-NH_2 groups in ABT could justify the biological activities observed for this species with gap values between 4.5933 and 4.8164 eV different from antiviral agents containing the C-NH_2 moiety, as amantadine and chloroquine whose gap values are around 4.3012-4.1116 eV. Finally, the presence of bands of monomer and of both dimers are predicted in the vibrational spectra and, hence, its completes assignments have been performed. The scaled force constants for the three studied species are also reported.

Keywords: *1-Aminobenzotriazole, molecular structure, harmonic force fields, vibrational analysis, DFT calculations.*

Introduction

1-Aminobenzotriazole (ABT) has been used from long time as an inhibitor of cytochrome P450 enzymes (Colby et al., 1995; Mugford et al., 1992; Emoto et al.,2003; Balani et al., 2004; Sun et al., 2011; Parrish et al., 2015; Watanabe et al., 2016; Shaik et al., 2017; Sun et al., 2020; Sodhi & Halladay, 2021), as reported by Ortiz de Montellano (2018). Few experimental and theoretical studies related only to two fused benzyls and triazole rings were found in the literature, however, combined crystalline structures obtained of benzotriazole rings with other rings or species have been recently published (Li et al., 2020; Karrouchi et al., 2023). N-H···O, O-H···N, and C-H···F hydrogen bonds interactions were determined in the crystal of 1*H*-benzotriazole and tetrafluoroterephthalic acid (Li et al., 2020) while three different C–H···N, O–H···N and C–H···O hydrogen bonds in the 5-((1H-benzo[d][1,2,3]triazol-1-yl)methyl)quinolin-8-ol (DD2) derivative were found (Karrouchi et al.,

2023). Obviously, in ABT these types of interactions also are expected due to the presence of similar groups, as in DD2 where these interactions were observed between two N atoms of triazole ring of one monomer with two H atoms of benzyl ring of other monomer (Karrouchi et al., 2023). Thus, dimers species should be structurally considered in these derivatives because the interactions have influence on the properties, reactivities and biological activities. All these antecedents evidence that the studies related to structures and properties of 1-Aminobenzotriazole are important not only to understand the mechanisms and sites of action of this important inhibitor of cytochrome P450 enzymes but also, to know reactivities and behaviour of ABT in different media and, in addition, to identify this species in different environments. Thus, the aims of this work are: (i) to optimize monomer and two possible dimers of ABT in gas phase and water by using B3LYP/6-311++G** calculations, (ii) to predict their properties, reactivities and behaviours in both environments (Becke, 1988; Yang & Parr, 1988; Miertus et al., 1981; Tomasi & Persico, 1994; Marenich et al., 2009), (iii) to perform the complete vibrational assignments of monomer and dimers of ABT using the harmonic force fields, normal coordinates analyses and transferable scaling factors (Pulay et al., 1983; Rauhut & Pulay, 1995; Sundius, 2002) and, finally (iv) to compute the scaled force constants of those species of ABT. Comparisons of experimental ^{1}H, ^{13}C-NMR, infrared and Raman of ABT with the corresponding predicted by calculations have confirmed the presence of monomer and both dimers of ABT (Online Spectral Database, N/A).

Material and methods

Structures of monomer and two possible dimers of ABT have been modelled with the *GaussView* program (Nielsen & Holder, 2008) while its optimizations in gas phase and water were performed with the Gaussian 09 program (Frisch et al., 2009). The optimized structures of monomer of ABT is shown in Figure 1. Here, two dimers were proposed because in one of them (dimer 1) the monomers are in the same positions while in the other one both monomers are in inverted positions (dimer 2), according to published article of DD2 (Karrouchi et al., 2023). The optimized structures of both dimers of ABT can be seen in Figure 2.

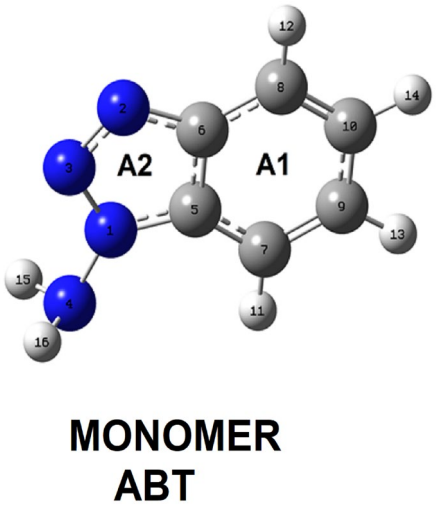

Figure 1. Structures of Monomer of 1 Amino-Benzotriazole (ABT) with Definitions of Rings and Atoms Labelling

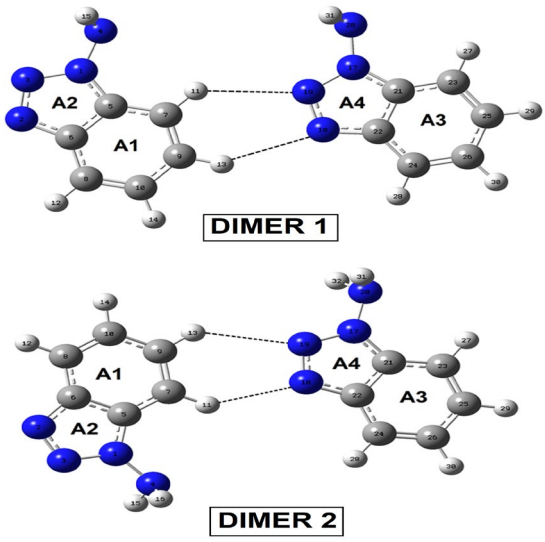

Figure 2. Structures of Dimers of 1 Amino-Benzotriazole (ABT) with Definitions of rings and atoms labelling. Intramolecular H-Bonds are Represented with Dashed Lines

In all calculations, the hybrid B3LYP/6-311++G** method was employed because this method generates better correlations to perform the complete vibrational analyses (Becke, 1988;) (Yang & Parr, 1988). Changes of volume of both species in the different media were predicted with the Moldraw program (Ugliengo, 1998). To investigate both species in water and to compute the solvation energies, the IEF-PCM and universal solvation method (SMD) were used (Miertus et al., 1981; Tomasi & Persico, 1994; Marenich et al., 2009). Atomic charges, topological and structural properties were calculated with the NBO 5.1 and AIM 2000 programs (Glendening et al. 1996; Bader, 1990; Biegler-Köning et al., 2001). Merz-Kollman (MK) charges were computed to calculate the molecular electrostatic potentials (MEP) while with the *GaussView* program were graphed the mapped MEP surfaces (Nielsen & Holder, 2008; Bredas, 2014). Reactivities and behaviours of monomer and dimer of ABT were estimated employing the frontier orbitals and the chemical potential, electronegativity, global hardness, global softness and global electrophilicity index descriptors (Karrouchi et al., 2023; Parr & Pearson, 1983; Parr et al., 1999). Vibrational assignments for monomer and dimers were performed at the same level of theory with the harmonic force fields (Pulay et al., 1983; Rauhut & Pulay, 1995; Sundius, 2002). Here, the normal internal coordinates of both triazole and benzyl rings were taken from reported work of DD2 (Karrouchi et al., 2023). In the dimers, only changes in the inter-monomers coordinates are observed. In these analyses, potential energy distribution (PED) contributions ≥ 10% were considered. The Raman spectra predicted in activities for monomer and the two dimers were transformed to intensities (Keresztury et al., 1993). The ^{1}H and ^{13}C NMR spectra of both species in aqueous solution were predicted with the GIAO method (Ditchfield, 1974). Finally, the electronic spectra for those species of ABT in aqueous solution were predicted using the Gaussian 09 program (Frisch et al., 2009).

Results and Discussion

Optimizations of Monomer and Dimers

First, in Figures 1 and 2 the optimized structures of monomer and both proposed dimers of ABT are presented, respectively while the calculated total and corrected by ZPVE energies, dipole moments and volumes of both species of ABT in the different media by using B3LYP/6-311++G** calculations are shown in Table 1.

Table 1. Calculated Total (E) and Corrected by ZPVE Energies (E_{ZPVE}), Dipole Moments (μ) and Volumes (V) of Monomer and Dimer of ABT in Gas Phase and Aqueous Solution by Using B3LYP/6-311++G Level of Theory. Permittivity's (ε) and Differences of Energy (ΔG) Values are Also Included**

B3LYP/6-311++G** Method							
MONOMER							
Medium	E (Hartrees)	E_{ZPVE}	μ(D)	V(Å^3)	ε	ΔG(kJ/Mol)	ΔG_{ZPVE}(kJ/Mol)
Gas	-451.3120	-451.1898	3.16	137.2	0		
Water	-451.3280	-451.2059	4.59	137.6	78.36	-41.97	-42.23
DIMER 1							
Medium	E (Hartrees)	E_{ZPVE}	μ(D)	V(Å^3)	ε	ΔG(kJ/Mol)	ΔG_{ZPVE}(kJ/Mol)
Gas	-902.6270	-902.3819	7.07	278.0	0		
Water	-902.6562	-902.4113	8.74	287.6	78.36	-76.59	-77.11
DIMER 2							
Medium	E (Hartrees)	E_{ZPVE}	μ(D)	V(Å^3)	ε	ΔG(kJ/Mol)	ΔG_{ZPVE}(kJ/Mol)
Gas	-902.6270	-902.3819	7.15	283.1	0		
Water	-902.6563	-902.4113	8.83	288.4	78.36	-76.85	-77.11

In the table the permittivity's and differences of energy (ΔG) values are included. Analysing the results, the E values of all species have most negative values than the E_{ZPVE} and the dipole moment values are higher in solution, as expected because the acceptors (N) and donor's groups (N-H) of H bonds are possibly hydrated in solution. Clear expansions of volumes are observed in solution for the three species. Note that E dimer 1 is the same than dimer 2 in both media but higher volume expansion presents the dimer 1 while higher dipole moment value is observed in the dimer 2. The energy (ΔG) values correspond to the differences of E in solution – E gas phase while ΔG_{ZPVE} is the differences between E_{ZPVE} in solution $-E_{ZPVE}$ gas phase. Note that ΔG_{ZPVE} have higher values than the corresponding to ΔG. The E values are corrected by zero-point vibrational energies (ZPVE) because the molecules present movements even in the zero K. Regarding the positions and orientations of dipole moment vectors of three species from Figures S1 to S3 (supporting material) we observed that in the monomer the magnitude of vector change few in solution while in this medium the vectors of both dimers change in significant form of magnitude and position but few changes in the directions and orientations are observed. Hence, the both dimeric species of ABT justify the higher volumes variations in solution (9.6/5.3 $Å^3$), as compared with the change observed in the monomer in this medium (0.4 $Å^3$).

Solvation Energies

In the above section, we observed that both monomer and dimers species of ABT are hydrated in aqueous solution due to the presence of donors (N-H) and acceptors (N) groups of H bonds which produce not only changes in the structures but also in volumes and, as a consequence different magnitudes and directions of the dipole moments vectors are observed. Hence, the solvation energies should be investigated in the two species in order to evaluate the different degrees of hydration of these species. Thus, from the difference between the corrected solvation energies by ZPVE ($\Delta G_{un}^{\#}$) and by the non-electrostatic terms (ΔG_{ne}) it is possible to calculate the corrected solvation energies (ΔG_c). Table 2 shows the corrected solvation energies by ZPVE and by the total non-electrostatic terms of monomer and dimers species of ABT in aqueous solution by using the B3LYP/6-311++G** method.

Table 2. Corrected Solvation Energies ($\Delta G_{C/ZPVE}$) and Uncorrected by ZPVE Energies (ΔG_{un}) and Volumes Variations (ΔV) of Monomer and Dimer of ABT in Aqueous Solution by Using the B3LYP/6-311++G Method. Units Expressed in kJ/mol**

B3LYP/6-311++G** Method					
MONOMER[a]					
Medium	ΔG_{un}	ΔG_{ne}	ΔG_C	ΔV($Å^3$)	$\Delta G_{C/ZPVE}$
Water	-41.97	9.97	-51.94	0.4	
	-42.23	9.97		0.4	-52.20
DIMER 1[a]					
Water	-76.59	19.52	-96.11	9.6	
	-77.11	19.52		9.6	-96.63
DIMER 2[a]					
Water	-76.85	19.60	-96.45	5.3	
	-77.11	19.60		5.3	-96.71
Oseltamivir[b]					
Water	-89.71	37.66	-127.37	-3.1	
Amantadine[c]					
Water	-15.21	7.86	-23.07	0.1	

Rimantadine[d]					
Water	-10.75	12.03	-22.78	0.2	

Note: [a]This work, [b] Vakili et al., (2021), [c] Brandán, (2021), [d] Iramain et al., (2022)

Hence, for the monomer ΔG_c= -51.94 kJ/mol is calculated as, $\Delta G_c = (\Delta G_{un}^{\#}) - (\Delta G_{ne})$ = -41.97 - 9.97 = -51.94 kJ/mol. For the dimer 1, ΔG_c= -96.11 kJ/mol and $\Delta G_{C/ZPVE}$= -96.63 kJ/mol. Here, the dimer 2 presents a higher value (ΔG= -76.85 kJ/mol). When these corrected values for ABT are compared with the ΔG_c values corresponding to antiviral agents, such as oseltamivir (-127.37 kJ/mol) (Vakili et al., 2021), amantadine or adamantadine (-23.07 kJ/mol) (Brandán, 2021) and rimantadine (-22.78 kJ/mol) (Iramain et al., 2022), where these two latter species are as free base, the values are very different from oseltamivir. Obviously, the different structures explain such differences (See Figure S4). In the three compared structures the donor common NH_2 group are bonded to C as C-NH_2 while in ABT the same donor group is bonded to N as N-NH_2. Besides, oseltamivir has other donor N-H group and other acceptors groups (O) in addition to N atoms and, for these reasons, a higher value in the solvation energy is expected in this antiviral species, as compared to amantadine and rimantadine. Probably, the higher value observed for ABT than amantadine and rimantadine is justified due to N atom bonded to NH_2 group because it has a lone pair that could be hydrated in solution. This way, a different biological property as inhibitor of cytochrome P450 enzymes in ABT is expected.

Structural Study

So far, the experimental structure of ABT was not reported yet and, taking into account that correlations between theoretical and experimental parameters are important to perform vibrational studies with a suitable structure we compared our results with the structure experimental determined for DD2 by using X-ray diffraction (Karrouchi et al., 2023). Hence, optimized parameters for monomer of ABT in gas phase and water by using the same level of theory are compared in Table 3 with the corresponding to that benzotriazole derivative by using the root-mean-square deviation values (RMSD). The structures of those two compounds can be seen in Figure S5 and the benzotriazole moiety common is indicated in red circle. Very good correlations are found for bond lengths and angles, with values of 0.082 Å for bond lengths and between 1.3 and 2.3 ° for bond angles in both media, respectively. Here, clearly the bond angles values in solution are slightly higher than in the gas phase due to the hydration while some signs changes are observed in the dihedral N4-N1-N3-N2, N4-N1-C5-C7, N4-N1-C5-C6, N3-N2-C6-C8, C5-C7-C9-H13, N2-C6-C8-C10, C7-C9-C10-H14 and C6-C8-C10-H14 angles which were not considered in the RMSD values. These dihedral angles are indicated with the # symbol in Table 3. The very good agreements in these parameters and, obviously, between the structures indicate that the optimized ones can be used in the vibrational analyses.

Table 3. Comparison of Calculated Geometrical Parameters for the Monomer of ABT in Gas Phase and Aqueous Solution by Using the B3LYP/6-311++G(d,p) Method with the Corresponding Experimental of C2 Conformer of 5-((1H-benzo[d][1,2,3]triazol-1-yl)methyl)Quinolin-8-ol (DD2)

B3LYP/6-311++G** Method[a]			Exp.[b]
Parameters	Gas Phase	Water	
Bond lengths (Å)			
N1-N3	1.366	1.354	1.351(5)
N1-C5	1.365	1.364	1.373(5)

N1-N4	1.388	1.391	1.442(5)
N3-N2	1.288	1.298	1.296(6)
N2-C6	1.381	1.378	1.378(6)
C5-C7	1.399	1.400	1.389(6)
C5-C6	1.405	1.404	1.377(6)
C7-H11	1.082	1.082	0.930
C7-C9	1.384	1.383	1.338(6)
C6-C8	1.402	1.404	1.411(7)
C9-H13	1.084	1.083	0.930
C9-C10	1.416	1.418	1.390(7)
C8-H12	1.083	1.083	0.930
C8-C10	1.382	1.382	1.382(8)
C10-H14	1.083	1.083	0.930
RMSD	**0.082**	**0.082**	
Bond angles (°)			
N3-N2-C6	108.6	108.4	109.9(3)
N3-N1-N4	122.7	123.0	120.5(3)
C5-N1-N4	126.6	126.4	129.5(3)
N1-N3-N2	108.9	109.0	109.6(4)
N3-N2-C6	108.6	108.4	107.2(4)
N1-C5-C7	134.1	133.8	133.3(4)
N1-C5-C6	103.2	103.5	103.4(3)
C7-C5-C6	122.5	122.5	123.3(4)
C5-C7-H11	121.5	121.8	122.2
C5-C7-C9	116.0	115.9	115.5(4)
H11-C7-C9	122.4	122.1	122.3
N2-C6-C5	108.6	108.3	109.9(4)
N2-C6-C8	130.7	130.8	130.7(4)
C5-C6-C8	120.6	110.7	119.5(4)
C7-C9-H13	119.1	119.1	117.7
C7-C9-C10	122.0	122.0	124.5(5)
C6-C8-H12	120.6	121.0	121.3
C6-C8-C10	117.2	117.0	117.5(5)
H12-C8-C10	122.1	121.9	121.2
C9-C10-C8	121.4	121.5	119.6(5)
C9-C10-H14	118.8	118.7	120.2
C8-C10-H14	119.7	119.6	120.2
RMSD	**1.3**	**2.3**	
Dihedral angles (°)			
C5-N1-N3-N2	0.0	0.0	1.3(5)
N4-N1-N3-N2#	-179.9	-179.9	178.9(4)
N3-N1-C5-C7	179.9	179.9	179.8(4)
N3-N1-C5-C6	-0.0	-0.0	-0.8(4)
N4-N1-C5-C7#	-0.0	-0.0	2.4(7)

N4-N1-C5-C6#	179.9	179.9	-178.2(4)
N1-N3-N2-C6	-0.0	-0.0	-1.1(5)
N3-N2-C6-C5	0.0	0.0	0.6(5)
N3-N2-C6-C8#	-179.9	-179.9	179.3(5)
N1-C5-C7-H11	0.0	-0.0	-0.3
N1-C5-C7-C9	180.0	179.9	179.7(4)
C5-C7-C9-H13	-179.9	-179.9	-179.6
C6-C5-C7-C9	0.0	0.0	0.4(6)
N1-C5-C6-N2	-0.0	-0.0	0.1(5)
N1-C5-C6-C8	-179.9	-179.9	-178.7(4)
C7-C5-C6-N2	179.9	179.9	179.6(4)
C7-C5-C6-C8	0.0	-0.0	0.8(7)
C5-C7-C9-H13#	-179.9	-179.9	179.3
C5-C7-C9-C10	0.0	-0.0	-0.7(7)
H11-C7-C9-H13	0.0	0.0	-0.6
H11-C7-C9-C10	180.0	179.9	179.3
N2-C6-C8-H12	0.0	0.0	-0.4
N2-C6-C8-C10#	-179.9	-179.9	179.7(5)
C5-C6-C8-H12	179.9	179.9	178.2
C5-C6-C8-C10	0.0	0.0	-1.8(7)
C7-C9-C10-C8	0.0	0.0	-0.4(8)
C7-C9-C10-H14#	-179.9	-179.9	179.6
H13-C9-C10-C8	179.9	179.9	179.6
H13-C9-C10-H14	0.0	0.0	-0.4
C6-C8-C10-C9	0.0	0.0	1.6(8)
C6-C8-C10-H14#	179.9	179.9	-178.4
H12-C8-C10-C9	-179.9	-179.9	-178.4
H12-C8-C10-H14	0.0	0.0	1.7
RMSD	**0.9**	**0.9**	

Note: [a]This work, Bold letter, RMSD values, #Indicate signs changes

NMR Study

Previously, we see the very good correlations in the geometrical parameters of monomer of ABT with the experimental structure reported for DD2. Now, we must see the correlations between the predicted NMR spectra of monomer and dimers of ABT in aqueous solution with the corresponding experimental ones (Online Spectral Database, N/A). Therefore, in Tables 4 and 5 are summarized the comparisons of predicted ^{1}H- and ^{13}C-NMR chemical shifts of those three species of ABT by using the GIAO and B3LYP/6-311++G** methods with the corresponding experimental obtained in $CDCl_3$ and Dimethyl sulfoxide-d_6 taken from Ref (Online Spectral Database, N/A).

Table 4. Observed and Calculated 1H Chemical Shifts (δ in ppm) for Monomer of ABT in Aqueous Solution at B3LYP/6-311++G Level of Theory**

Atoms	B3LYP/6-311++G**					Exp.[b]
	Monomer[a]	Dimer 1		Dimer 2		
11-H	7.73	11-H	8.11	11-H	8.25	7.50
12-H	8.17	12-H	8.07	12-H	8.10	7.90
13-H	7.55	13-H	8.02	13-H	7.99	7.40
14-H	7.45	14-H	7.58	14-H	7.49	7.25
15-H	4.97	15-H	5.04	15-H	5.00	5.9
16-H	4.97	16-H	5.04	16-H	5.05	5.9
		27-H	7.91	27-H	7.80	7.50
		28-H	8.27	28-H	8.25	7.90
		29-H	7.61	29-H	7.66	7.40
		30-H	7.43	30-H	7.52	7.25
		31-H	5.14	31-H	5.10	5.9
		32-H	5.13	32-H	5.08	5.9
RMSD	**0.57**		**0.57**		**0.59**	

Note: [a]This work GIAO/B3LYP/6-311++G** Ref. to TMS, [b]Online Spectral Database (N/A)

Table 5. Observed and Calculated 13C Chemical Shifts (δ in ppm) for Monomer of ABT in Aqueous Solution at B3LYP/6-311++G Level of Theory**

Atoms	B3LYP/6-311++G**				Experimental[b]
	Monomer[a]	Dimer 1		Dimer 2	
5-C	138.52	5-C	138.46	138.53	133
6-C	150.83	6-C	150.43	150.44	144
7-C	113.00	7-C	114.59	114.65	110
8-C	125.40	8-C	124.72	124.39	119
9-C	131.77	9-C	133.55	132.58	126
10-C	127.72	10-C	128.36	127.83	124
		21-C	137.63	138.43	133
		22-C	150.38	151.07	144
		23-C	113.57	113.92	110
		24-C	126.24	125.58	119
		25-C	132.20	132.32	126
		26-C	128.11	128.17	124
RMSD	**5.39**		**5.65**	**5.60**	

Note: [a]This work GIAO/B3LYP/6-311++G** Ref. to TMS, [b]Online Spectral Database (N/A)

The comparisons are evaluated by means of the RMSD values and presented in the same tables. Table 4 shows for the ^{1}H nucleus a RMSDs value of 0.57 ppm for the monomer and dimer 1 while for dimer 2 the value is 0.59 ppm indicating that formation of dimeric species can also be seen in solution. For the ^{13}C nucleus the value increase from 5.39 ppm for the monomer to 5.65 and

5.60 ppm. Note that despite of different experimental used solvents the better correlation is observed for the ^{1}H nucleus because the hybrid B3LYP/6-311++G** method generate best results than the C atoms. Moreover, the few differences found for the three species could indicate the presence of dimeric species. Hence, the higher rmsds values observed could be associated to that the theoretical calculations were performed in different solvents and to the dimeric species formed. These reasonable correlations indicate that the structure of monomer and dimers are suitable to perform their vibrational studies.

Atomic Charges, Molecular Electrostatic Potential (MEP) and Bond Orders

The presence of acceptors (N) and donor's (N-H) groups of H bonds in ABT are important not only to explain the properties and activities observed in this interesting benzotriazole derivative but also the mechanisms and sites of reaction. For these reasons, in this section the atomic MK and NPA charges, MEP and bond orders (BO) have been predicted and analysed. Hence, two different atomic charges were calculated only on the acceptors (N) and donor's (N-H) groups of H bonds in ABT in both environments, they are atomic MK and NPA charges (Glendening et al., 1996; Bredas, 2014). Thus, in Table S1 are presented the atomic charges, MEP and BOs on those N1, N2, N3, N4, H15 and H16 atoms of ABT involved in H bonds. Besides, Figure S6 shows the variations observed on calculated MK and NPA charges on N and H atoms corresponding to ABT in both media by using the B3LYP/6-311++G** method. N1, N2 and N3 atoms belong to triazole moiety while N4 and H atoms to NH_2 groups. Hence, those three atoms are acceptors of H bonds while the other one's donors of H bonds. Regarding Figure S3 we observed that the MK charges on N1 in both media present positive values while the NPA corresponding to these atoms show negative values, as also are observed on N2 and N3. Both charges evidence the most negative values on N4, as expected because these atoms are linked to the most labile H15 and H16 atoms. This way, the two charges show positive values on those two H atoms.

If now from Table S1 are evaluated the MEP values computed from MK charges, it is observed higher values on the N atoms while the less negative MEP values are observed on H atoms due to these two atoms of NH_2 groups are most labile. Few variations on MEP values are observed when change the media from gas phase to the solution. However, when the mapped MEP surfaces of monomer in the two environments and of dimers in gas phase are shown in Figures S7 and S8 the energies values of monomer slightly increase from 0.0535 a.u in gas phase to 0.0543 a.u in solution while for both dimers the values decrease in solution. Hence, the nucleophilic sites of red colours are clearly observed on the N2 and N3 while the electrophilic sites with strong blue colours are observed on the two H atoms because these have less negative MEP values and are most labile. Analysing the mapped MEP surface for the dimers in gas phase it is observed from Figure S8 a slight higher energy for the dimer 2 (± 0.060 a.u.) than dimer 1 (± 0.0593 a.u.) and an, increases of blue coloration, but the red colour decrease, as a consequence of H bonds formation. The regions with green colours correspond to inert sites.

Evaluating the bond orders (BO) totals by atom, expressed as Wiberg bond index from Table S1, we can see that the N4 present lower values (2.824-2.821), as expected because these atoms are most labile and, for these reasons, they are less bonded to triazole rings while N1 have the higher values (3.610-3.617) because they are most bonded to triazole moieties. These studies support the existence of two clear nucleophilic and electrophilic regions in ABT associated to the acceptors and donor's groups de H bonds.

NBO and AIM Calculations

In the structure experimental reported for DD2 by using X-ray diffraction (Karrouchi et al., 2023) are observed C-H···N bonds between two monomers in inverted positions. These interactions are also expected in dimers of ABT studies because these species containing donor and acceptor groups of H bonds, and, for these reasons, NBO and AIM calculations were performed for monomer and dimers with the

NBO 3.1 and AIM 2000 programs (Glendening et al., 1996; Bader, 1990; Biegler-Köning et al., 2001). In the NBO calculations, the donor-acceptor energy interactions were computed for the three species with the Second-Order Perturbation Theory Analysis of Fock Matrix in NBO Basis and by using B3LYP/6-311++G** calculations. These main delocalizations energies for the monomer of ABT in both environments are shown in Table S2 while in Table S3 can be seen those predicted for both dimers. The results from Table S2 for the monomer show four different types of interactions which are: $\pi \rightarrow \pi^*$, $n \rightarrow \pi^*$, $n \rightarrow \sigma^*$ and $\pi^* \rightarrow \pi^*$ transitions and, where $\pi \rightarrow \pi^*$ and $\pi^* \rightarrow \pi^*$ present the higher energy values in the two considered media. Evaluating the total energy value is clear that the monomer in solution has a slight higher stability with a value of 2110.95 kJ/mol while in gas phase the value is 1932.87 kJ/mol. When the calculated main delocalization energies for both dimers 1 and 2 of ABT in the two environments are analysed from Table S3, it is observed those same interactions but with higher energy values where, as in the monomer, the $\pi \rightarrow \pi^*$ and $\pi^* \rightarrow \pi^*$ interactions present the higher energy values in the two considered media. Hence, both dimers are stable in gas phase because the total energy values are for dimers 1 and 2 are respectively 6110.91 and 6196.64 kJ/mol while in solution the values decrease respectively at 5115.69 and 5223.54 kJ/mol. In solution are observed H bonds elongations which decreases the stability of the corresponding monomers. Thus, the dimer 2 (6196.64 kJ/mol) is more stable than dimer 1 because it presents a slightly higher total energy value. The decreasing of energies for the dimers in solution could be attributed to higher solvation energy values (-96.11 kJ/mol), as compared with the monomer (-51.94 kJ/mol) (see Table 2). The values of both dimers are lower for the dimer 1 and, hence, the dimer 2 could be present in the solid phase, as observed in DD2 (Karrouchi et al., 2023).

Studying the H bonds interactions for monomer and dimers of ABT in the two environments through the topological properties with the AIM 2000 program the electron density, the Laplacian values and the $|\lambda 1|/\lambda 3$ ratio are calculated in the bond critical points (BCPs) and in the ring critical points (RCPs) (Bader, 1990; Biegler-Köning et al., 2001). Thus, in Table S4 are presented those properties together with the distances of new H bonds for the dimers. The $|\lambda 1|/\lambda 3$ ratios are calculated with the eigenvalues of the Hessian matrix $(\lambda 1, \lambda 2, \lambda 3)$. From these values it is possible to see that if the interaction is ionic or polar covalent interactions the ratio $\lambda 1/\lambda 3 < 1$ and $\nabla^2\rho(r) > 0$ (closed-shell interaction). Regarding the graphics obtained of the molecular model for the monomer of ABT in gas phase from Figure S9 it is observed the typical RCP1 and RCP2 due to the benzyl or phenyl (A1) and triazole (A2) rings. hence, there is not observed new H bonds interactions while when these graphics are obtained for the dimers in gas phase in Figures 3 and 4 two H bonds are shown.

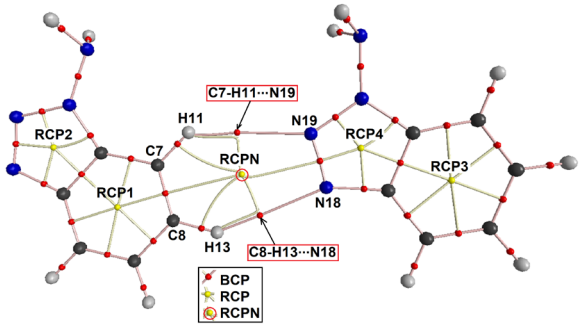

Figure 3. Details of the Molecular Models for the Dimer 1 of ABT in Gas Phase by Using the B3LYP/6-311++G Method Showing the Geometries of All Their Bond Critical Points (BCPs) and Ring Critical Points (RCPs)**

For dimer 1, Figure 3 shows the formations of C7-H11···N19 and C8-H13···N18 interactions which generate a new RCP named RCPN. In the same way, for dimer 2 from Figure 4 are observed two C7-H11···N18 and C9-H13···N19 interactions. Moreover, the H bonds distances between those atoms for the two dimers increase in solution as a consequence of hydrations. Note that the atoms involved in the new interactions change due to the different positions of monomers in the respective dimers. Regarding Table S4 we observed that the

topological properties of dimer 2 present higher values than dimer 1 due to the lower distances between the H and N atoms. These NBO and AIM results show that dimer 2 present a slight higher stability in both media than dimer 1 and, for these reasons, this species will be present in the solid phase, as experimentally was observed for DD2 (Karrouchi et al., 2023).

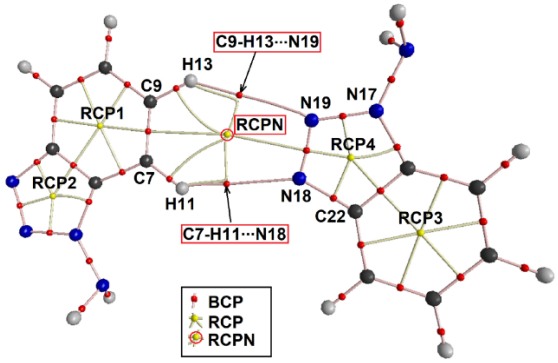

Figure 4. Details of the Molecular Models for the Dimer 2 of ABT in Gas Phase by Using the B3LYP/6-311++G Method Showing the Geometries of All Their Bond Critical Points (BCPs) and Ring Critical Points (RCPs)**

Frontier Orbitals Studies

Frontier orbitals are appreciated factors to predict reactivities and behaviours of a species in diverse media calculating the gap values from the differences between the HOMO-LUMO and with which can be computed different descriptors (Parr & Pearson, 1983; Parr et al., 1999; Vakili et al., 2021; Brandán, 2021; Iramain et al., 2022). In this case, the behaviours of monomer and dimers of ABT were predicted in the two media together with the chemical potential (μ), electronegativity (χ), global hardness (η), global softness (S) and global electrophilicity index (ω) descriptors. Hence, in Table S5 are shown the results for monomer and dimers of ABT compared with the C2 conformer of DD2 (Karrouchi et al., 2023) and with antivirals agents such as, oseltamivir (Vakili et al., 2021), adamantadine (Brandán, 2021) and chloroquine (Romano et al., 2020) in aqueous solution at the same level of theory. Note that the equations used are also presented in the table. Evaluating the gap values, we observed that the monomer in gas phase presents a lower gap value than the value in solution and, hence, it presents a higher reactivity in gas phase while the dimer 2 in both media are more reactive than dimer 1. Comparing these values with reported for the mentioned antiviral agents, the monomer is more reactive than oseltamivir (5.1892/5.1947 eV) while the dimer 2 of ABT evidence a higher reactivity than the monomer and oseltamivir, however, adamantadine (Brandán, 2021) and chloroquine (Romano et al., 2020) have lower values than ABT. Possibly, the presence of dimer 2 and of two N-NH_2 groups in ABT justify the biological activities observed for this species whose gap values are between 4.8817 and 4.5933 eV different from antiviral agents containing the C-NH_2 moiety, as amantadine whose gap values are around 4-3012-4.2994 eV. In reference to the descriptors, in the two dimers of ABT in both media are observed high (ω) values than the monomer while the antiviral amantadine presents the higher reactivity and the lower (ω) value. Hence, we not observed anything correlation between gap value and (ω), however, a lower global hardness (η) is related to lower reactivity or lower gap value.

The participations of all orbitals including of the benzotriazole rings in the HOMO-LUMO for monomer of ABT in both media is very clear, as observed in Figures S10 while for the dimers in both media from Figure S11 (only presented in gas phase because is the same in solution) shows that the participations of each monomer in the dimer are partial. Hence, changes in the HOMOs and LUMOs of each dimer are observed in Figure S11. These characteristics of HOMO-LUMO of both dimeric species could justify their biological properties as an inhibitor of cytochrome P450 enzymes.

Vibrational Study

B3LYP/6-311G* calculations optimized the monomer and the two dimers of ABT with C_1 symmetries. In the monomer with 16 atoms are expected 42 normal vibration modes while for the two dimers with 32 atoms are expected 90. The experimental ATR-IR spectrum of ABT in

the solid phase compared with the corresponding predicted for the three species in the gas phase are shown in Figure 5 while comparisons of Raman spectra are observed in Figure 6 (Online Spectral Database, N/A). The Raman spectra show better correlations with the experimental one due to the corrections from activities to intensities (Keresztury et al., 1993). The harmonic force fields were obtained using transferable scaling factors and normal internal coordinates and PED contributions ≥ 10% in order to perform the complete assignments of three species of ABT (Pulay et al., 1983; Rauhut & Pulay, 1995; Sundius, 2002).

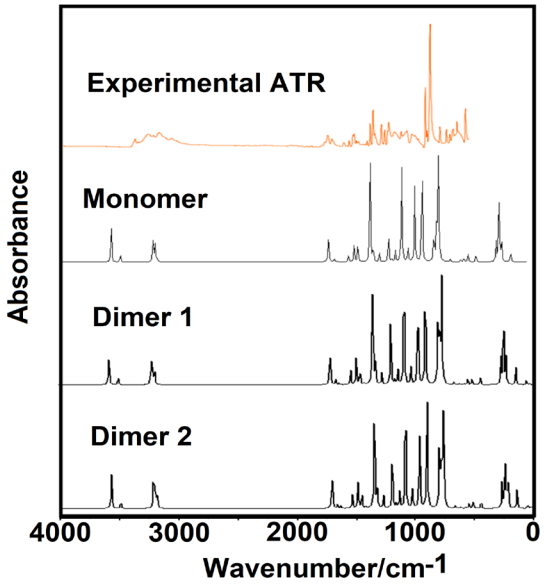

Figure 5. Experimental Infrared Spectrum of 1 Amino-Benzotriazole (ABT) Compared with the Corresponding Predicted for Monomer and Dimers by Using the Hybrid B3LYP/6-311++G Method**

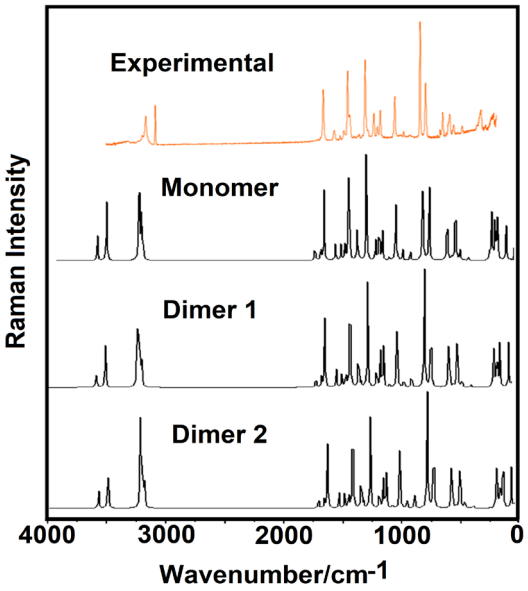

Figure 6. Experimental Raman Spectrum of 1 Amino-Benzotriazole (ABT) Compared with the Corresponding Predicted for Monomer and Dimers by Using the Hybrid B3LYP/6-311++G Method**

Thus, in Table 6 are summarized observed and calculated wavenumbers and assignments for monomer and dimers of ABT in the gas phase by using B3LYP/6-311++G** calculations. The positions and intensities predicted for both dimers are practically the same in the region of higher wavenumbers with some differences in the assignments in the 1700-40 cm^{-1} region related to NH_2 groups and to inter-monomers observed. Here, some discussions of assignments are presented for some groups by regions.

Table 6. Observed and Calculated Wavenumbers (cm-1) and Assignments for Monomer and Dimers of ABT in Gas Phase by Using B3LYP/6-311++G Method**

Experimental[a]		B3LYP/6-311++G** Method[a]					
		MONOMER		DIMER 1		DIMER 2	
IR	Raman	SQM[b]	Assignments[a]	SQM[b]	Assignments[a]	SQM[b]	Assignments[a]
		3413	ν_aNH_2	3414	ν_aNH_2(N20)	3414	ν_aNH_2(N20)
3343w				3408	ν_aNH_2(N4)	3412	ν_aNH_2(N4)
		3338	ν_aNH_2	3338	ν_sNH_2(N20)	3338	ν_sNH_2(N20)
3314w				3334	ν_sNH_2(N4)	3337	ν_sNH_2(N4)

3227w	3226w	3073	νC7-H11	3079	νC7-H11	3075	νC7-H11
3179w	3179w			3074	νC23-H27	3074	νC23-H27
3132w	3131w			3069	νC24-H28	3069	νC24-H28
3088sh	3069vs	3068	νC8-H12	3066	νC8-H12	3065	νC8-H12,νC10-H14
				3055	νC26-H30	3056	νC9-H13
		3053	νC10-H14	3055	νC9-H13	3054	νC26-H30
3020w				3042	νC25-H29	3041	νC25-H29
2988w	2996s	3040	νC9-H13	3041	νC10-H14	3040	νC10-H14
1667sh		1623	δNH_2	1622	δNH_2(N4)	1622	δNH_2(N20)
1643m				1622	δNH_2(N20), $wagNH_2$(N20)	1622	δNH_2(N4),$wagNH_2$(N4)
1608w	1594s	1594	νC5-C7	1594	νC21-C23	1593	νC21-C23
1608w	1594s			1592	νC5-C7	1592	νC5-C7
1608w	1594s			1568	νC5-C6,νC6-C8	1569	νC21-C22,νC22-C24
1502w	1504w	1568	νC5-C6,νC6-C8	1568	νC21-C22	1568	νC5-C6,νC6-C8
1476w		1478	νC8-C10	1479	νC24-C26	1479	νC24-C26
1456w	1451w			1478	νC8-C10	1477	νC8-C10,νN1-C5
		1433	βC8-H12,βC7-	1433	βC24-H28,βC23-H27	1433	βC24-H28,βC23-H27
1419m	1424w			1431	βC8-H12,βC7-H11	1431	βC8-H12,βC7-H11
1408m	1394vs	1403	νN1-C5	1404	νN1-C5	1404	νN1-N4,βR_1(A2)
1393w	1394vs			1403	νN17-C21	1403	νN17-
1372w	1377m	1364	νC9-C10,νC5-C6	1364	νC9-C10,νC8-C1	1364	νC25-C26,νC24-C26
1341w	1338w			1363	νC25-C26,νC24-C26	1363	νC9-C10,νC7-C9
1309w	1312sh	1301	ϱNH_2	1302	ϱNH_2(N4)	1303	ϱNH_2(N4)
1296w	1298w			1301	ϱNH_2(N20)	1299	ϱNH_2(N20)
1274s		1295	νN2-N3	1293	νN2-N3	1293	νN2-N3
1246vs	1247vs			1292	νN18-N19	1292	νN18-N19
1233sh				1285	βC23-H27	1286	βC7-H11
		1284	βC7-H11	1285	βC7-H11,βC8-H12	1285	βC23-H27
1228m	1225sh			1226	νN18-C22	1227	νN18-C22
1228m	1225sh	1225	νN2-C6	1225	νN2-C6	1225	νN2-C6
1172s	1172m			1157	βC9-H13,βC7-	1155	βC9-H13
1144m	1146w	1152	βC9-H13,νC7-	1154	βC25-H29,νC23-C25	1153	βC25-H29,νC23-C25
1118sh	1120m	1121	βC8-H12,βC10-	1122	βC24-H28,βC26-H30	1122	βC24-H28,βC26-H30
1118sh	1120m			1118	βC8-H12,βC10-H14	1118	βC8-H12,βC10-H14
1106s				1102	βR_1(A1),βC7-H11	1103	βR_1(A1),νC5-C6
1098sh	1086vw	1099	βR_1(A1),βC7-	1100	βR_1(A3),βC23-H27	1099	βR_1(A3),βC23-H27
1057m	1059vw			1048	νN17-N19	1047	νN17-N19
1040sh	999s	1039	νN1-N3	1041	νN1-N3	1042	νN1-N3
1000m	999s			1005	γC9-H13	1000	γC9-H13
957sh	955w			986	γC25-H29,γC26-H30	985	γC25-H29,γC26-H30
		984	γC9-H13,γC10-	983	νC9-C10	984	νC9-C10
945m		983	νC9-C10	983	νC25-C26	983	νC25-C26
				956	γC8-H12,γC10-H14	955	γC10-H14,γC8-H12
934sh	924w	950	γC8-H12	951	γC24-H28	951	γC24-H28
				930	βR_1(A3), βR_2(A4)	930	βR_1(A3),βR_2(A4)
903m		929	βR_1(A1),βR_2(A2)	929	βR_1(A1),βR_2(A2)	928	βR_1(A1),βR_2(A2)

872m	873vw			862	γC7-H11	864	γC7-H11
848w	850vw	852	γC7-H11	853	γC23-H27	852	γC23-H27
		834	wagNH$_2$	839	wagNH$_2$(N4)	834	wagNH$_2$(N4)
783vs	790vs			834	wagNH$_2$(N20)	831	wagNH$_2$(N20)
783vs	790vs	771	wagNH$_2$,βR$_3$(A1)	771	wagNH$_2$(N4)	770	wagNH$_2$(N20)
770sh	770sh			771	νC22-C24	769	wagNH$_2$(N4),βR$_3$(A1)
				766	γC9-H13,γC8-H12	765	γC9-H13,γC8-H12
753sh	751sh	756	γC9-	758	τR$_1$(A3), γC25-H29	756	γC25-H29,τR$_1$(A3)
				744	τR$_1$(A3)	745	τR$_1$(A1),τR$_1$(A2)
		740	τR$_1$(A1),τR$_1$(A2)	744	τR$_1$(A1), τR$_1$(A2)	740	τR$_1$(A3),τR$_1$(A4)
742vs	742s			726	νN17-N20	726	νN17-N20,νN1-N4
727sh		724	νN1-N4	726	νN1-N4	725	νN1-N4,νN17-N20
659m	646w			639	τR$_2$(A4),τR$_1$(A4)	638	τR$_2$(A4)
620w	625w	637	τR$_2$(A2)	636	τR$_2$(A2)	637	τR$_2$(A2)
596m	602m			595	βR$_1$(A2)	595	βR$_1$(A4), βR$_1$(A2)
596m	602m	594	βR$_1$(A2)	594	βR$_1$(A4)	594	βR$_1$(A2),βR$_1$(A4)
568w	550sh			551	τR$_2$(A1),τR$_2$(A2)	552	τR$_2$(A1),τR$_2$(A2)
568w	550sh	550	τR$_2$(A2),τR$_2$(A1)	550	τR$_2$(A3), τR$_2$(A4)	550	τR$_2$(A3),τR$_2$(A4)
546sh				532	βR$_3$(A3)	532	βR$_3$(A3)
538m	537m	530	βR$_3$(A1)	531	βR$_3$(A1)	531	βR$_3$(A1)
505m	506w			497	βR$_2$(A3)	497	βR$_2$(A3)
489sh	476w	495	βR$_2$(A1)	495	βR$_2$(A1)	495	βR$_2$(A1)
431s	442w			427	τR$_3$(A1),τR$_2$(A1)	427	τR$_3$(A1),τR$_2$(A1)
417sh		424	τR$_3$(A1),τR$_2$(A1)	425	τR$_3$(A3),τR$_2$(A3)	425	τR$_3$(A3),τR$_2$(A3)
	281m	272	γN1-N4,τR$_2$(A2)	272	γN17-N20,τR$_2$(A4)	272	γN1-N4,τR$_2$(A2)
	281m			271	γN1-N4τR$_2$(A2)	271	γN17-N20,τR$_2$(A4)
	242w			262	βN17-N20	261	βN17-N20
	242w	260	βN1-N4	261	βN1-N4	261	βN1-N4
	215sh			227	ButC21-C22	226	ButC21-C22
	215sh	223	ButC6-C5	225	ButC6-C5	223	ButC6-C5
	194sh	204	τwNH$_2$	211	τwNH$_2$(N20)	206	τwNH$_2$(N20)
	176m			205	τwNH$_2$(N4)	196	τwNH$_2$(N4)
		137	γN1-N4	136	γN17-N20	136	γN1-N4
				134	γN1-N4	135	γN17-N
				43	γ$_a$N-H···N	40	γ$_a$N-H···N
				36	ν$_a$N-H···N	34	ν$_a$N-H···N
				20	δN-H···N	23	δN-H···N
				16	τ$_w$N-H···N, τ$_w$N-	16	τ$_w$N-H···N
				14	ν$_s$N-H···N	15	ν$_s$N-H···N
				12	τ$_w$N-H···N,τ$_w$N-	9	τ$_w$N-H···N

Abbreviations: ν, stretching; β, deformation in the plane; γ, deformation out of plane; wag, wagging; τ, torsion; ρ, rocking; τw, twisting; δ, deformation; a, antisymmetric; s, symmetric; A1, A3, Benzyl; A2, A4; Triazole rings; [a]This work, [b]From SQMFF/B3LYP/6-311++G** method.

Band Assignments. 4000-2000 cm^{-1} region

In monomer and dimers, the NH_2 and C-H stretching (ν) modes are predicted practically in the same positions. The ν_a NH_2 modes are assigned to the IR band at 3343 cm^{-1} while the symmetric mode at 3314 cm^{-1}, as reported for similar species (Karrouchi et al., 2023; Vakili et al., 2021; Brandán, 2021; Iramain et al., 2022). IR and Raman bands between 3227 and 2988 cm^{-1} are related to νC-H modes of three species of ABT because these modes in DD2 containing benzotriazole moiety were assigned to IR bands between 3100 and 2850 cm^{-1} (Karrouchi et al., 2023).

Band Assignments. 1800-1000 cm^{-1} region.

This region is typical of deformation (δ), wagging and rocking modes corresponding to NH_2 groups, in-plane or rocking (β) and out-of-plane (γ) deformations of CH and νC=C, νC=N, νC-C modes (Karrouchi et al., 2023; Vakili et al., 2021; Brandán, 2021; Iramain et al., 2022). Hence, the shoulder and the IR band respectively at 1667 and 1643 cm^{-1} are assigned to δNH_2 modes of three species while the IR and Raman bands between 1608 and 1394 cm^{-1} are assigned to νC=C and νC=N modes with double or partial double bond character of three species while other νC-C and νC-N modes between 1377 and 1000 cm^{-1} are assigned to those vibration modes of simple bonds. In DD2 (Karrouchi et al., 2023), the βCH modes are assigned between 1507 and 1100 cm^{-1} while the γCH deformations between 600 and 900 cm^{-1}. In the three species of ABT these modes are assigned between 1233 and 1120 900 cm^{-1}.

Band Assignments. 1000-10 cm^{-1} region.

In this region are expected twisting and wagging modes of CH and NH_2 together with νC-C modes and other skeletal modes, such as γCH deformations and deformations and torsions of two rings. Thus, NH_2 wagging and twisting modes are predicted to 839/769 and 211/196 cm^{-1}, hence, these modes are assigned to the bands between 790/770 and 194/176 cm^{-1}, respectively. The remains skeletal and deformation (β_R) and torsion (τ_R) rings modes are assigned according to predicted by SQM calculations, as detailed in Table 6.

Force Constants

The application of the SQMFF approach and the Molvib program have permitted the calculations of scaled force constants for monomer and dimers of ABT in the two media (Pulay et al., 1983; Rauhut & Pulay, 1995; Sundius, 2002). These factors are presented in Table 7 compared with reported for the C2 conformer of DD2 in the same media (Karrouchi et al., 2023).

Table 7. Scaled Internal Force Constants for ABT in Gas Phase and Water Solution Compared with Reported for the C2 Conformer of 5-((1H-benzo[d][1,2,3]triazol-1-yl)methyl)quinolin-8-ol (DD2) in the Same Media by Using the B3LYP/6-311++G Method**

B3LYP/6-311++G** method								
Force constant	Monomer		Dimer 1		Dimer 2		DD2[b]	
	GAS	Water					GAS	Water
f(νNH₂)	6.31	6.30	6.32	6.30	6.33	6.32		
f(νC-H)A1,A3	5.14	5.15	5.14	5.16	5.16	5.16	5.09	5.14
f(νC-C)A1	6.28	6.28	6.28	6.29	6.29	6.29	6.27	6.28
f(νC-N)A2,A4	5.82	5.91	5.84	5.93	5.85	5.91	7.89	7.69
f(νN-N)A2,A4	5.79	5.73	5.80	5.74	5.80	5.74	5.98	5.96
f(δNH₂)	0.85	0.79	0.85	0.80	0.84	0.79		

Note: Units are mdyn $Å^{-1}$ for stretching and mdyn Å rad^{-2} for angle deformations. [a]This work, [b]Karrouchi et al., 2023.

Here, it is necessary a clarification for those $f(\nu N\text{-}N)_{A2,A4}$ and $f(\nu C\text{-}H)_{A1,A3}$ force constants related to the benzotriazole rings (A1 and A3 correspond to benzyl ring while A2 and A4 to triazole ring). Hence, the $f(\nu C\text{-}H)_{A1,A3}$ force constants related to the C-H bonds of benzyl rings have the same values in the three species of ABT and in the different media. Regarding the $f(\nu NH_2)$ force constants associated to NH_2 groups of monomer and dimers in both media it is observed that practically present the same values in gas phase and short changes undergoes in solution, as was also observed in the antiviral oseltamivir (6.42/6.32 mdyn $Å^{-1}$), adamantadine (6.31/6.20 mdyn $Å^{-1}$) and rimantadine (6.42 mdyn $Å^{-1}$) (Vakili et al., 2021; Brandán, 2021; Iramain et al., 2022). Moreover, these same behaviours are observed in the $f(\nu N\text{-}N)_{A2,A4}$ force constants associated to triazole rings of three species of ABT. These diminishing in the $f(\nu NH_2)$ and $f(\nu N\text{-}N)_{A2,A4}$ force constants values indicate that these groups are hydrated in solution, as expected because NH_2 is a donor group of H bonds while the N atoms are acceptors of H bonds. For these reasons, in the DD2 species which contain a benzotriazole ring the same differences are observed (Karrouchi et al., 2023). Different behaviours in the $f(\nu C\text{-}N)_{A2,A4}$ force constants values of monomer and dimers are observed because their values increase in solution but the values practically are similar in the three species. These studies support the presence of the three species of ABT in the two media.

Electronic Spectra

The predicted electronic spectrum of monomer and dimers of ABT in aqueous solution by using the B3LYP/6-311++G** method are compared in Figure S12 with the experimental of 1,2,3-Benzotriazole in aqueous solution taken between 200 and 350 nm (Breuer et al., 2012). Two bands with different intensities can be observed in the experimental spectrum where the most intense is located at c.a. 210 nm and other less intense at 277 nm. In the monomer, two intense bands at 190 and 240 nm with a shoulder at 260 nm are observed but in the dimers the intense band is at 240 nm and the shoulder at 260 nm and the other band of lower λ it is not observed in these species. The bands observed are associated to $\pi\rightarrow\pi^*$, $n\rightarrow\pi^*$ and $\pi^*\rightarrow\pi^*$ transitions predicted for these species by NBO calculations. Note that the band intense at 190 nm in the monomer is not predicted in the dimers. The experimental UV spectrum of 1,2,3-benzotriazole show the presence clear of monomer and dimers of this benzotriazole derivative and, hence, both bands should be observed in ABT and, as a consequence the three species of ABT are present in the experimental ^{1}H- and ^{13}C-NMR, IR and Raman spectra.

Conclusions

The following conclusions were obtained of this investigation:

Structural, topological and vibrational properties of monomer and two dimers (1 and 2) of 1-Aminobenzotriazole (ABT) have been studied combining hybrid B3LYP/6-311++G** calculations with the experimental ^{1}H-, ^{13}C-NMR, FT-IR and FT-Raman spectra.

B3LYP/6-311++G** calculations predict C-H···N interactions of dimeric species, as was experimentally observed in benzotriazole derivatives.

NBO and AIM calculations suggest that dimer2 with inverted positions of its monomers could be present in the solid phase because it evidence higher stabilities in both media.

Frontier orbitals studies support a higher reactivity of dimer 2 of ABT than the monomer and dimer 1. This way, the presence of dimer 2 containing N-NH_2 groups in ABT could justify the biological activities observed for this species with gap values between 4.5933 and 4.8164 eV different from antiviral agents containing the C-NH_2 moiety, as amantadine and chloroquine whose gap values are around 4.3012-4.1116 eV.

The presence of bands of monomer and of both dimers are predicted in the vibrational spectra and, hence, its completes assignments of monomer and dimers have been performed. The scaled force constants are also reported for the three studied species.

The presence of monomer and dimer species of ABT are predicted by using their UV spectra, as was experimentally observed in benzotriazole derivatives.

Supplementary Information

Figures S1-S12 (Appendix 1) and TablesS1-S5 (Appendix 2).

Acknowledgements

The authors would like to thank Prof. Tom Sundius for his permission to use MOLVIB

Author Contribution

ME. Manzur and PG. Cataldo performed the calculations MA. Iramain and MV. Castillo: prepared figures and tables. SA. Brandán: wrote the main manuscript text. All authors reviewed the manuscript.

Funding

This work was supported with grants from CIUNT Project N°. 26/D714 (Consejo de Investigaciones, Universidad Nacional de Tucumán).

Conflicts of Interest

The authors declare no conflict of interest.

References

Bader, R.F.W. (1990). *Atoms in molecules.* A Quantum Theory. Oxford University Press, Oxford, ISBN: 0198558651 25.

Balani, S.K., Li, P., Nguyen, J., Cardoza, K., Zeng, H., Mu, D.X., Wu, J.-T., Gan, L.-S. & Lee, F.W. (2004). Effective dosing regimen of 1-aminobenzotriazole for inhibition of antipyrine clearance in guinea pigs and mice using serial sampling. *Drug Metabolism and Disposition, 32*(10), 1092-1095. https://doi.org/10.1124/dmd.104.000349

Becke, A.D. (1988). Density-functional exchange-energy approximation with correct asymptotic behavior. *Physical Review A, 38*, 3098–3100. https://doi.org/10.1103/physreva.38.3098

Biegler-Köning, F., Schönbohm, J. & Bayles, D. (2001). AIM2000; A program to analyze and visualize atoms in molecules. *Journal of Computational Chemistry, 22*(5), 54526. https://doi.org/10.1002/1096-987X(20010415)22:5<545::AID-JCC1027>3.0.CO;2-Y

Brandán, S.A. (2021). Normal internal coordinates Force fields and vibrational study of Species Derived from Antiviral adamantadine, *International Journal of Quantum Chemistry, 121*(2), e26425. https://doi.org/10.1002/qua.26425

Bredas, J.L. (2014). Mind the gap! Material Horizons, 1(1), 17-19. https://doi.org/10.1039/C3MH00098B

Breuer, D., Fisher, P. & Hansen, K. (2012). The Mak collection for Occupational Health and Safety. In *The MAK-Collection for Occupational Health and Safety*. https://doi.org/10.1002/3527600418.am1002497e0010b

Colby, H.D., Abbott, B., Cachovic, M., Debolt, K.M. & Mico, B.A. (1995). Inactivation of adrenal cytochromes P450 by 1-aminobenzotriazole: Divergence of in vivo and in vitro actions. *Biochemical Pharmacology, 49*(8), 1057-1062. https://doi.org/10.1016/0006-2952(95)98501-Y

Ditchfield, R. (1974). Self-consistent perturbation theory of diamagnetism. I. A gage-invariant LCAO (linear combination of atomic orbitals) method for NMR chemical shifts. *International Journal at the Interface Between Chemistry*

and Physics, 27, 714–722. https://doi.org/10.1080/00268977400100711

Emoto, C., Murase, S., Sawada, Y., Jones, B.C. & Iwasaki, K. (2003). In Vitro Inhibitory Effect of 1-Aminobenzotriazole on Drug Oxidations Catalyzed by Human Cytochrome P450 Enzymes: A Comparison with SKF-525A and Ketoconazole. *Drug Metabolism and Pharmacokinetics, 18*(5), 287-295. https://doi.org/10.2133/dmpk.18.287

Frisch, J., Trucks, G.W., Schlegel, H.B. & Scuseria, G.E. (2009). *Gaussian 09, Revision A.02, M.* Wallingford CT: Gaussian, Inc.

Glendening, E.D., Badenhoop, J.K., Reed, A.D., Carpenter, J.E. & Weinhold, F. (1996). *NBO 3.1.* Theoretical Chemistry Institute, University of Wisconsin, Madison, WI 24.

Iramain, M.A., Ruiz Hidalgo, J., Sundius, T. & Brandán, S.A. (2022). A Combined Study on Structures and Vibrational Spectra of Antiviral Rimantadine using SQMFF and DFT calculations. *Heliyon, 8*, e10102. https://doi.org/10.1016/j.heliyon.2022.e10102

Karrouchi, K., Himmi, B., Brandán, S.A., Sert, Y., Kawther, A.A., Dege, N., Cinar, E.B., El Louzi, A. & Bougrin, K. (2023). A quinoline-benzotriazole derivative: Synthesis, crystal structure and characterization by using spectroscopic, DFT and molecular docking methods. *Results in Chemistry, 5*, 100916. https://doi.org/10.1016/j.rechem.2023.100916

Keresztury, G., Holly, S., Besenyei, G., Varga, J., Wang, A.Y. & During, J.R. (1993). Vibrational spectra of monothiocarbamates-II. IR and Raman spectra, vibrational assignment, conformational analysis and ab initio calculations of S-methyl-N,N-dimethylthiocarbamate. *Spectrochimica Acta Part A: Molecular and Biomolecular Spectroscopy, 49,* 2007–2026. https://doi.org/10.1016/S0584-8539(09)91012-1

Li, F., Zheng, Z., Xia, S. & Yu, L. (2020). Synthesis, co-crystal structure, and DFT calculations of a multicomponent co-crystal constructed from 1*H*-benzotriazole and tetrafluoroterephthalic acid. *Journal of Molecular Structure, 1219*(5), 128480. https://doi.org/10.1016/j.molstruc.2020.128480

Marenich, A.V., Cramer, C.J.& Truhlar, D.G. (2009). Universal solvation model based on solute electron density and a continuum model of the solvent defined by the bulk dielectric constant and atomic surface tensions. *Journal of Physical Chemistry B, 113,* 6378–6396. https://doi.org/10.1021/jp810292n

Miertus, S., Scrocco, E. & Tomasi, J. (1981). Electrostatic interaction of a solute with a continuum. Chem Phys, 55, 117-129. https://doi.org/10.1016/0301-0104(81)85090-2

Mugford, C.A., Mortillo, M., Mico, B.A. & Tarloff, J.B. (1992). 1-Aminobenzotriazole-induced destruction of hepatic and renal cytochromes P450 in male Sprague-Dawley rats. *Fundamental and Applied Toxicology, 19*(1), 43-49. https://doi.org/10.1016/0272-0590(92)90026-E

Nielsen, A.B. & Holder, A.J. (2008). *Gauss View 5.0, User's Reference.* Pittsburgh, PA: GAUSSIAN Inc.

Online Spectral Database. (N/A). Quick access to millions of NMR, IR, Raman, UV-Vis, and Mass Spectra. Retrieved from https://spectrabase.com/spectrum

Ortiz de Montellano, P.R. (2018). 1-Aminobenzotriazole: A Mechanism-Based Cytochrome P450 Inhibitor and Probe of Cytochrome P450 Biology. Medicinal Chemistry, 8(3), 1-73. https://doi.org/10.4172/2161-0444.1000495

Parr, R.G. & Pearson, R.G. (1983). Absolute hardness: companion parameter to absolute electronegativity. *Journal of American Chemistry Society, 105*, 7512–7516. https://doi.org/10.1021/ja00364a005

Parr, R.G., Szentpaly, L.V. & Liu, S. (1999). Electrophilicity Index. *Journal of American Chemistry Society,* 121, 1922-1924. https://doi.org/10.1021/ja983494x

Parrish, K.E., Mao, J., Chen, J., Jaochico, A., Ly, J., Ho, Q., Mukadam, S. & Wright, M. (2016). In vitro and in vivo characterization of CYP

inhibition by 1-aminobenzotriazole in rats. *Biopharm & Drug Disposition, 37*(4), 200-211. https://doi.org/10.1002/bdd.2000

Pulay, P., Fogarasi, G., Pongor, G., Boggs, J.E. & Vargha, A. (1983). Combination of theoretical ab initio and experimental information to obtain reliable harmonic force constants. Scaled quantum mechanical (QM) force fields for glyoxal, acrolein, butadiene, formaldehyde, and ethylene. *Journal of American Chemistry Society, 105*, 7073. https://doi.org/10.1021/ja00362a005

Rauhut, G. & Pulay, P. (1995). Transferable scaling factors for density functional derived vibrational force fields. *Journal of Physical Chemistry, 99*, 3093–3099. https://doi.org/10.1021/j100010a019

Romano, E., Issaoui, N., Manzur, M.E. & Brandán, S.A. (2020). Properties and Molecular docking of Antiviral to COVID-19 Chloroquine combining DFT calculations with SQMFF approach, *International Journal of Current Advanced Research, 9*(8A), 22862-22876. https://doi.org/10.1016/j.jksus.2020.101248

Shaik, A.N., LeDuc, B.W. & Khan, A.A. (2017). Characterization of 1-Aminobenzotriazole and Ketoconazole as Novel Inhibitors of Monoamine Oxidase (MAO): An In Vitro Investigation. *European Journal of Drug Metabolism and Pharmacokinetics, 42*(5), 827-834. https://doi.org/10.1007/s13318-017-0401-6

Sodhi, J.K. & Halladay, J.S. (2021). Case Study 9: Probe-Dependent Binding Explains Lack of CYP2C9 Inactivation by 1-Aminobenzotriazole (ABT). *Methods in Molecular Biology, 2342*, 765-779. https://doi.org/10.1007/978-1-0716-1554-6_28

Sun, J., Xia, J., Zhao, X. & Liu, P. (2020). Effects of 1-aminobenzotriazole on the growth and physiological characteristics of Tamarix chinensis cuttings under salt stress. *Journal of Forestry Research, 32*(4), 1-11. https://doi.org/10.1007/s11676-020-01215-6

Sun, Q., Harperm T,W., Dierks, E.A., Zhang, L., Chang, S., Rodrigues, A.D. & Marathe, P. (2011). 1-Aminobenzotriazole, a known cytochrome P450 inhibitor, is a substrate and inhibitor of N-acetyltransferase. *Drug Metabolism and Disposition: the Biological Fate of Chemicals, 39*(9), 1674-1679. https://doi.org/10.1124/dmd.111.039834

Sundius, T. (2002). Scaling of ab initio force fields by MOLVIB. *Vibrational Spectroscopy, 29,* 89-95. http://dx.doi.org/10.1016/S0924-2031(01)00189-8

Tomasi, J. & Persico, J. (1994). Molecular interactions in solution: an overview of methods based on continous distributions of the solvent. *Chemistry Review, 94*, 2027–2094. https://doi.org/10.1021/cr00031a013

Ugliengo, P. (1998). *MOLDRAW Program.* University of Torino, Dipartimento Chimica IFM, Torino, Italy.

Vakili, M., Romano, E., Darugar, V. & Brandán, S.A. (2021). Behaviours of antiviral Oseltamivir in different media: DFT and SQMFF calculations. *Journal of Molecular Modeling, 27*, 357. https://doi.org/10.1007/s00894-021-04962-3

Watanabe, A., Mayumi, K., Nishimura, K. & Osaki, H. (2016). In vivo use of the CYP inhibitor 1-aminobenzotriazole to increase long-term exposure in mice. *Biopharm & Drug Disposition, 37*(6), 373-378. https://doi.org/10.1002/bdd.2020

Yang, W.C. & Parr, R.G. (1988). Development of the Colle-Salvetti correlation-energy formula into a functional of the electron density. *Physical Review B, 37*, 785-789. https://doi.org/10.1103/physrevb.37.785

Appendix 1

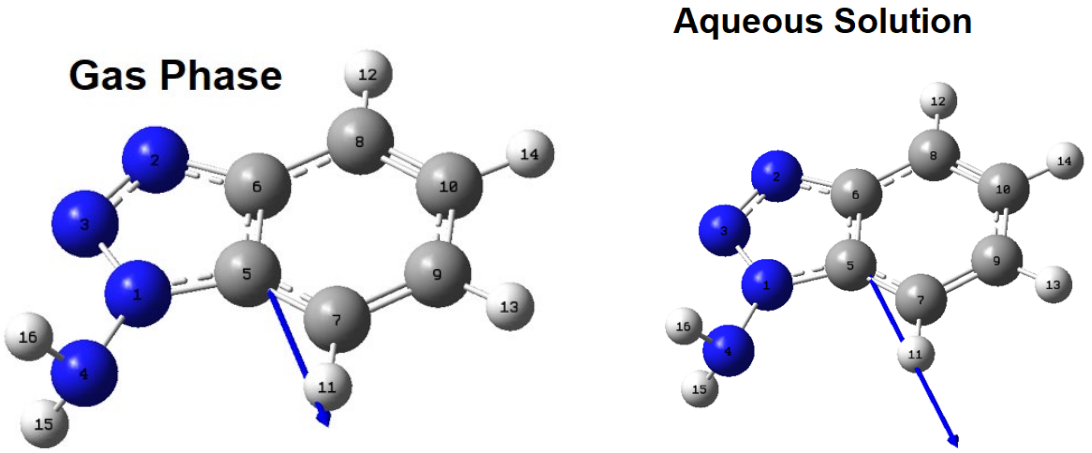

Figure S1. Orientations, Magnitudes and Directions of Dipole Moment Vectors of Monomer of ABT:(a) in Gas Phase (Upper) and (b) in Aqueous Solution (Bottom) by Using the B3LYP/6-311++G** Method

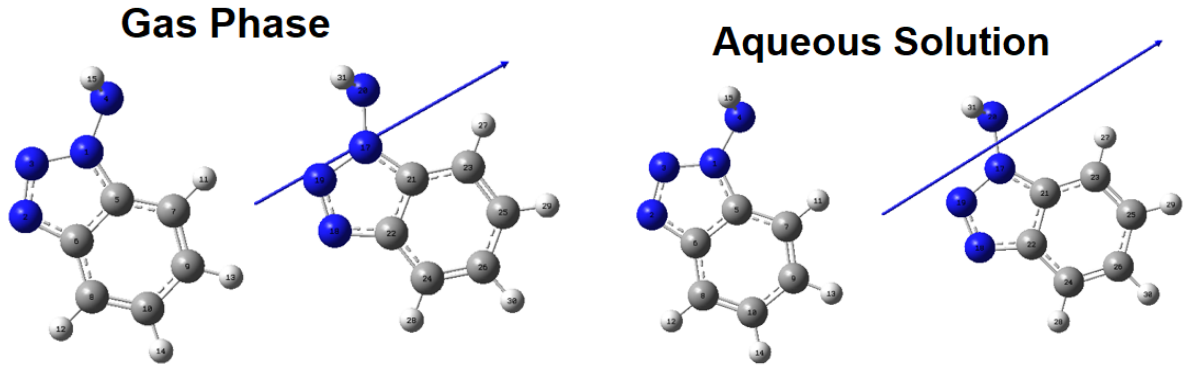

Figure S2. Orientations, Magnitudes and Directions of Dipole Moment Vectors of Dimer 1 of ABT:(a) in Gas Phase (Upper) and (b) in Aqueous Solution (Bottom) by Using the B3LYP/6-311++G** Method

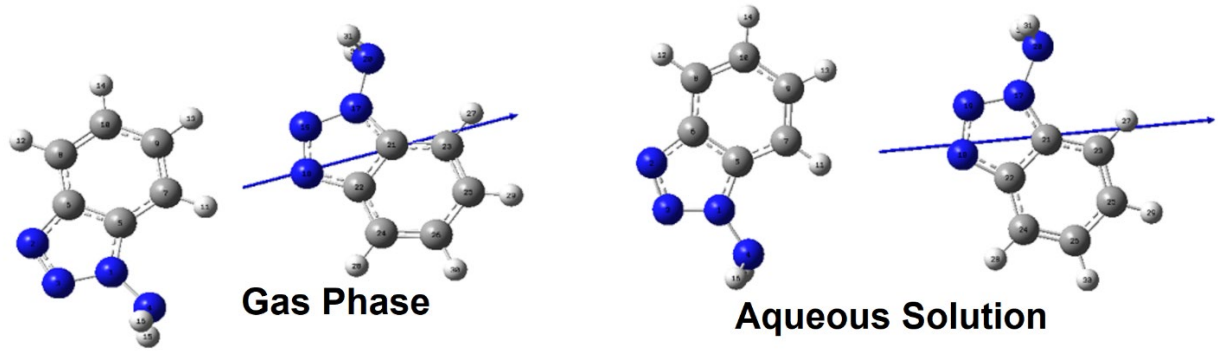

Figure S3. Orientations, Magnitudes and Directions of Dipole Moment Vectors of Dimer 2 of ABT:(a) in Gas Phase (Upper) and (b) in Aqueous Solution (Bottom) by Using the B3LYP/6-311++G** Method

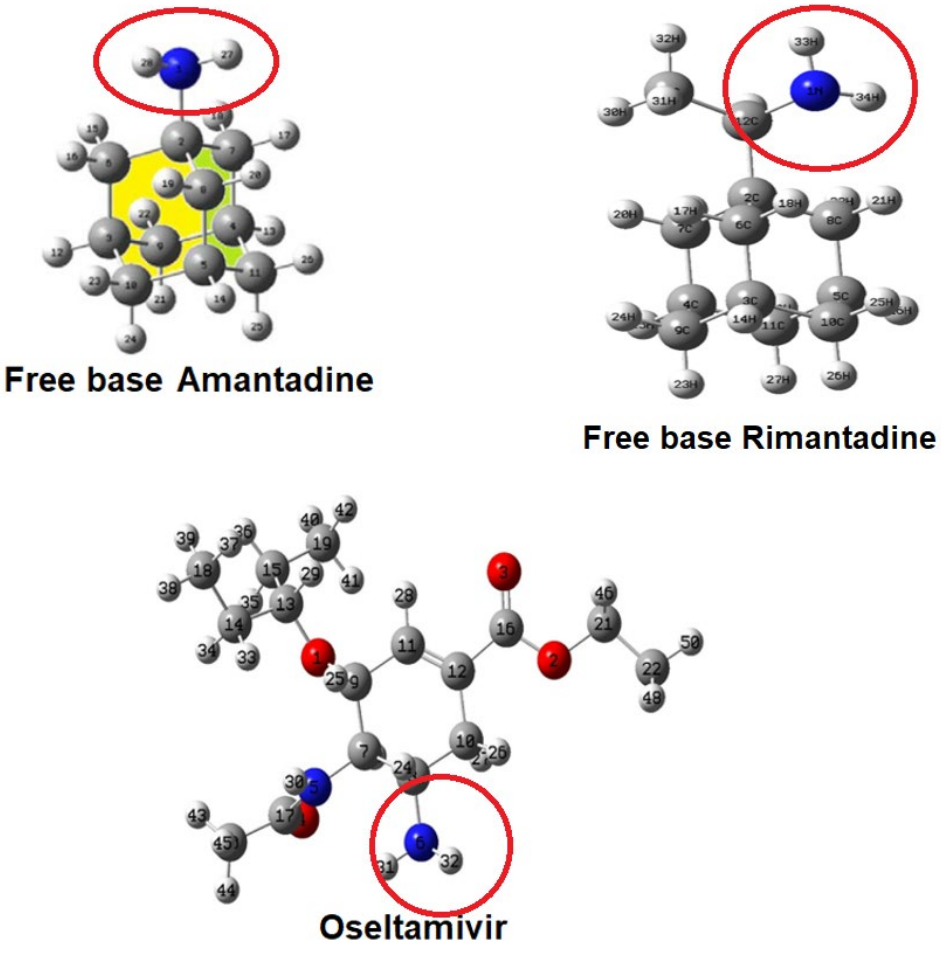

Figure S4. Optimized Structures of Antiviral Amantadine, Oseltamivir and Rimantadine Agents in Gas Phase with the Atoms Labelling by Using the B3LYP/6-311++G(d,p) Method. In Red Circle are Observed the Common C-NH2 Group

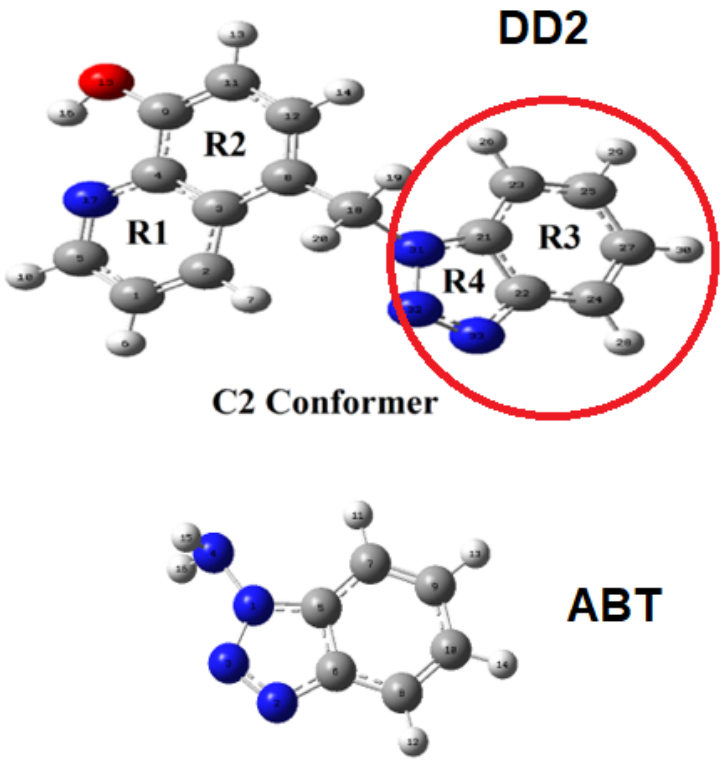

Figure S5. Optimized Structure of ABT in Gas Phase with the Atoms Labelling by Using the B3LYP/6-311++G(d,p) Method Compared with the Corresponding Experimental for the C2 Conformer of 5-((1H-benzo[d][1,2,3]triazol-1-yl)methyl)quinolin-8-ol (DD2)

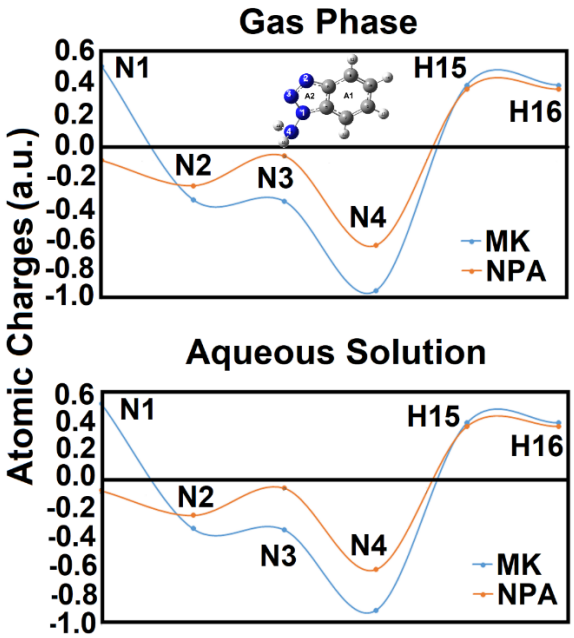

Figure S6: Variations Observed on Calculated MK and NPA Charges on N and H Atoms Corresponding to ABT in Both Media by Using the B3LYP/6-311++G** Method. The N Atoms Belong to Triazole Moiety while the H Atoms to NH2 Groups

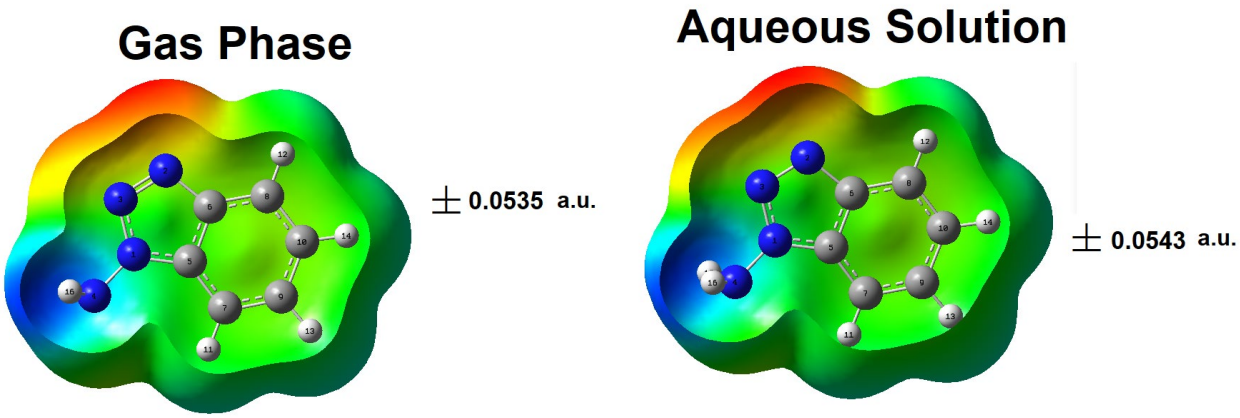

Figure S7. Calculated Electrostatic Potential Surface on the Molecular Surfaces of Monomer of ABT in Gas Phase and Aqueous Solution by Using the B3LYP/6-311++G** Method. Isodensity Value of 0.005

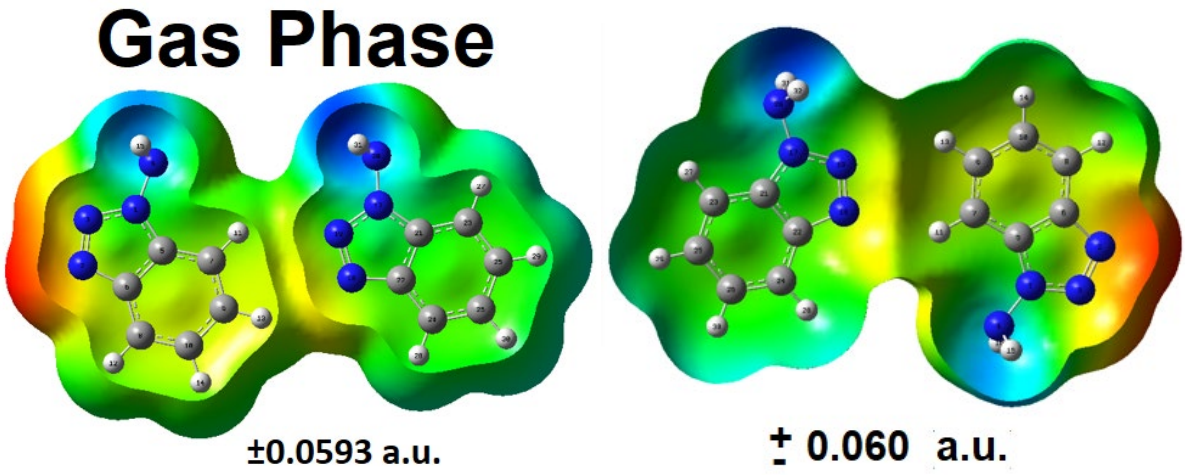

Figure S8. Calculated Electrostatic Potential Surface on the Molecular Surfaces of Dimer 1 (Upper) and Dimer 2 (Bottom) of ABT in Gas Phase by Using the B3LYP/6-311++G** Method. Isodensity Value of 0.005

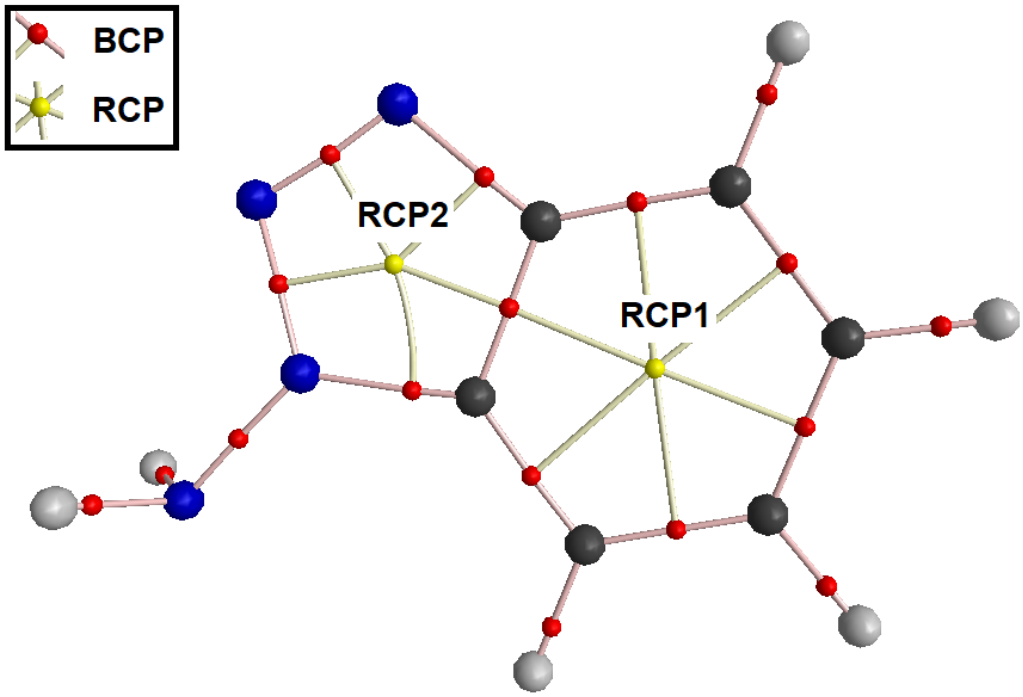

Figure S9. Details of the Molecular Models for the Monomer of ABT in Gas Phase by Using the B3LYP/6-311++G** Method Showing the Geometries of All Their Ring Critical Points (RCPs).

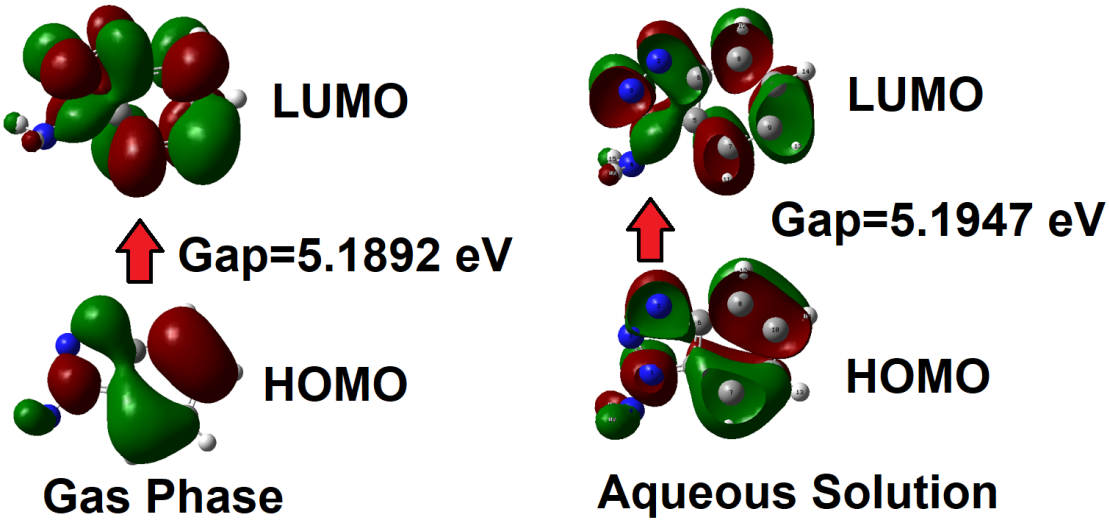

Figure S10. Comparisons Between the Frontier Orbitals HOMO-LUMO of Monomer of ABT in Gas Phase and Aqueous Solution by Using the B3LYP/6-311++G** Method

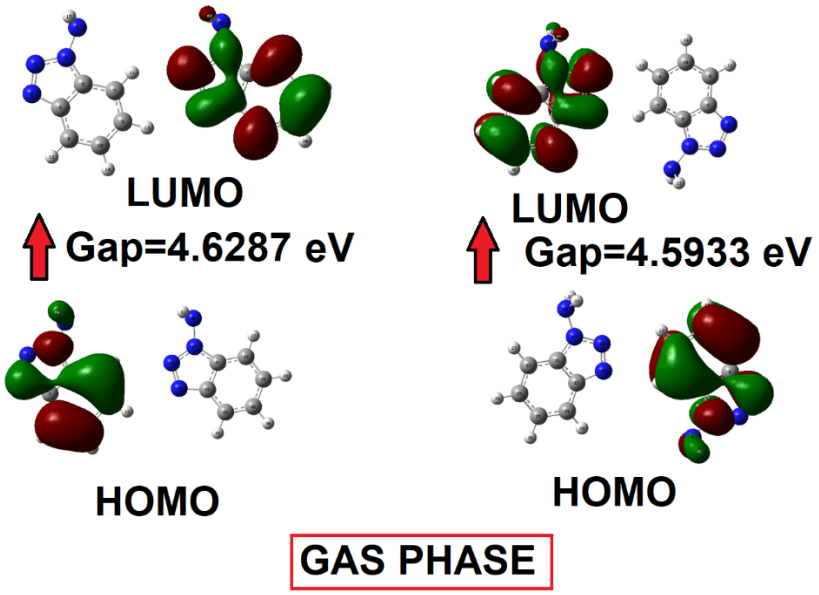

Figure S11. Comparisons Between the Frontier Orbitals HOMO-LUMO of Dimers 1 (Left) and 2 (right) of ABT in Gas Phase by Using the B3LYP/6-311++G** Method

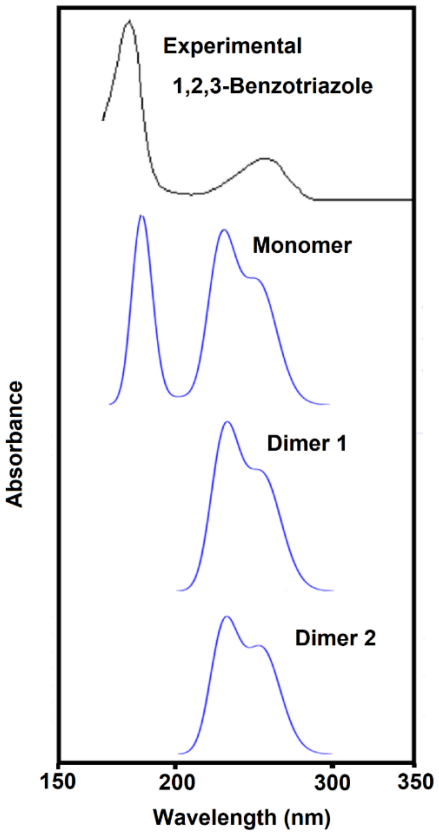

Figure S12. Experimental Electronic Spectrum of 1,2,3-Benzotriazole in Ethanol Solvent Compared with the Corresponding Predicted for Monomer and Dimer of ABT in Aqueous Solution by Using the B3LYP/6-311++G** Method

Appendix 2

Table S1. Merz-Kollman and NPA Charges (a.u.), Molecular Electrostatic Potentials (MEP) (a.u.) and Bond Orders, Expressed as Wiberg Indexes for ABT in Gas Phase and Aqueous Solution by Using B3LYP/6-311++G** Calculations

	GAS PHASE				AQUEOUS SOLUTION			
Atoms	MK	NPA	MEP	BO	MK	NPA	MEP	BO
N1	0.512	-0.081	-18.278	3.610	0.523	-0.075	-18.276	3.617
N2	-0.328	-0.241	-18.377	3.106	-0.336	-0.245	-18.378	3.098
N3	-0.339	-0.054	-18.340	3.082	-0.345	-0.057	-18.341	3.081
N4	-0.903	-0.617	-18.337	2.824	-0.900	-0.617	-18.336	2.821
H15	0.392	0.366	-1.012	0.869	0.391	0.367	-1.011	0.869
H16	0.392	0.366	-1.012	0.869	0.391	0.367	-1.011	0.869

Table S2. Main Delocalization Energies (in kJ/mol) for Monomer of ABT in Gas Phase and Aqueous Solution by Using B3LYP/6-311++G** Calculations

Delocalization[a]	B3LYP/6-311++G** Method[a]	
	Gas	Water
*πN2-N3 →π*C5-C6*	57.31	59.27
*πC5-C6 →π*N2-N3*	117.54	119.55
*πC5-C6→ π*C7-C9*	66.63	66.59
*πC5-C6→ π*C8-C10*	73.94	72.23
*πC7-C9→ π*C5-C6*	84.27	82.81
*πC7-C9→ π*C8-C10*	69.01	68.97
*πC8-C10→ π*C5-C6*	71.10	71.19
*πC8-C10→ π*C7-C9*	82.18	80.80
$\Delta E_{\pi\rightarrow\pi^*}$	**621.98**	**621.40**
*LP(1)N1→ π*C5-C6*	150.02	150.06
*LP(1)N1→ π*N2-N3*	0.00	188.64
$\Delta E_{LP\rightarrow\pi^*}$	**150.02**	**338.71**
*LP(1)N4→ σ*N1-N3*	46.36	45.19
$\Delta E_{LP\rightarrow\sigma^*}$	**46.36**	**45.19**
*π*N2-N3→ π*C5-C6*	171.05	164.69
*π*C5-C6→ π*C8-C10*	943.47	940.96
$\Delta E_{\pi^*\rightarrow\pi^*}$	**1114.51**	**1105.65**
ΔE_{TOTAL}	**1932.87**	**2110.95**

[a]This work

Table S3. Main Delocalization Energies (in kJ/mol) for Dimers 1 and 2 of ABT in Gas Phase and Aqueous Solution by Using B3LYP/6-311++G** Calculations

Delocalization[a]	B3LYP/6-311++G** Method[a]			
	DIMER 1		DIMER 2	
	Gas	Water	Gas	Water
*πN2-N3 →π*C5-C6*	56.64	58.56	56.93	58.77
*πC5-C6 →π*N2-N3*	120.22	120.55	119.80	120.34
*πC5-C6→ π*C7-C9*	64.16	65.33	64.92	65.71
*πC5-C6→ π*C8-C10*	73.36	71.94	73.82	72.36
*πC7-C9→ π*C5-C6*	88.07	84.90	86.74	84.27
*πC7-C9→ π*C8-C10*	71.06	70.10	72.40	70.93
*πC8-C10→ π*C5-C6*	71.14	71.31	70.77	70.93
*πC8-C10→ π*C7-C9*	80.30	80.01	79.29	79.25
*πN18-N19→ π*C21-C22*	56.85	58.81	56.85	58.94
*πC21-C22→π*N18-N19*	119.67	120.18	119.80	120.09
*πC21-C22→π*C23-C25*	59.57	66.25	59.73	66.21
*πC21-C22→π*C24-C26*	72.82	71.94	72.94	72.02
*πC23-C25→π*C21-C22*	84.90	83.18	84.77	83.14
*πC23-C25→π*C24-C26*	69.22	69.05	69.26	69.14
*πC24-C26→π*C21-C22*	71.48	71.35	71.52	71.35
*πC24-C26→π*C23-C25*	73.53	80.80	73.32	80.72
$\Delta E_{\pi\rightarrow\pi^*}$	**1232.97**	**1244.26**	**1232.85**	**1244.18**
*σN17-N20→ σ*C26-H30*	121.39	0.00	121.43	0.00
*σN20-H31→ σ*C25-H29*	0.00	0.00	43.56	0.00
*σN20-H31→ σ*C26-H30*	284.37	0.00	284.20	0.00
*σN20-H32→ σ*C25-C26*	47.23	0.00	0.00	0.00
*σN20-H32→ σ*C26-H30*	397.56	0.00	400.07	0.00
$\Delta E_{\sigma\rightarrow\sigma^*}$	**850.55**	**0.00**	**849.25**	0.00
*LP(1)N1→ π*C5-C6*	147.55	149.14	148.10	149.56
*LP(1)N1→ π*N2-N3*	178.03	188.60	179.32	189.35
*LP(1)N17→ π*N18-N19*	0.00	189.19	0.00	189.77
*LP(1)N17→ π*C21-C22*		150.02		
$\Delta E_{LP\rightarrow\pi^*}$	**325.58**	**676.95**	**327.42**	**528.69**
*LP(1)N4→ σ*N1-N3*	45.48	45.14	45.94	45.31
*LP(1)N20→ σ*N17-N19*	46.52	45.35	46.40	45.39
$\Delta E_{LP\rightarrow\sigma^*}$	**92.00**	**90.50**	**92.34**	**90.71**
*π*N2-N3→ π*C5-C6*	166.78	0.00	166.49	162.02
*π*C5-C6→ π*C7-C9*	879.14	1125.26	919.64	1138.13
*π*C5-C6→ π*C8-C10*	894.69	912.37	996.18	989.11
*π*N18-N19→ π*C21-C22*	164.27	162.23	163.02	162.14
*π*C21-C22→π*C23-C25*	312.58	0.00	292.35	0.00
*π*C21-C22→π*C24-C26*	836.50	904.13	861.12	908.56
*π*C24-C26→π*C23-C25*	355.84	0.00	295.99	0.00
$\Delta E_{\pi^*\rightarrow\pi^*}$	**3609.81**	**3103.98**	**3694.79**	**3359.97**
ΔE_{TOTAL}	**6110.91**	**5115.69**	**6196.64**	**5223.54**

[a]This work

Table S4. Analysis of the Bond Critical Points (BCPs) and Ring Critical Point (RCPs) for ATPO in Gas Phase and in Ethanol Solution by Using B3LYP/6-311++G Calculations**

B3LYP/6-311++G** Method							
MONOMER							
GAS PHASE							
Parameter#	RCP1	RCP2					
ρ(r)	0.0214	0.0543					
$\nabla^2\rho(r)$	0.1569	0.4332					
$\|\lambda1\|/\|\lambda3\|$	0.1725	0.2503					
AQUEOUS SOLUTION							
Parameter#	RCP1	RCP2					
ρ(r)	0.0214	0.0546					
$\nabla^2\rho(r)$	0.1566	0.4344					
$\|\lambda1\|/\|\lambda3\|$	0.1726	0.2527					
DIMER 1							
GAS PHASE							
Parameter#	RCP1	RCP2	RCP3	RCP4	RCPN	H11···N19	H13···N18
ρ(r)	0.0215	0.0542	0.0215	0.0544	0.0023	0.0052	0.0058
$\nabla^2\rho(r)$	0.1568	0.4324	0.1569	0.4332	0.0120	0.0158	0.0169
$\|\lambda1\|/\|\lambda3\|$	0.1738	0.2502	0.1734	0.2511	0.1444	0.1803	0.1883
Distances						2.812	2.765
AQUEOUS SOLUTION							
Parameter#	RCP1	RCP2	RCP3	RCP4	RCPN	H11···N19	H13···N18
ρ(r)	0.0214	0.0545	0.0214	0.0546	0.0002	0.0006	0.0003
$\nabla^2\rho(r)$	0.1568	0.4344	0.1566	0.4344	0.0001	0.0003	0.0001
$\|\lambda1\|/\|\lambda3\|$	0.1727	0.2527	0.1729	0.2526	0.0947	0.1243	0.1176
Distances						3.806	4.126
DIMER 2							
GAS PHASE							
Parameter#	RCP1	RCP2	RCP3	RCP4	RCPN	H11···N18	H13···N19
ρ(r)	0.0215	0.0542	0.0215	0.0544	0.0022	0.0068	0.0042
$\nabla^2\rho(r)$	0.1568	0.4325	0.1568	0.4332	0.0108	0.0198	0.0129
$\|\lambda1\|/\|\lambda3\|$	0.1736	0.2496	0.1736	0.2510	0.1460	0.1899	0.1718
Distances						2.699	2.899
AQUEOUS SOLUTION							
Parameter#	RCP1	RCP2	RCP3	RCP4	RCPN	H11···N18	H13···N19
ρ(r)	0.0214	0.0545	0.0214	0.0546	0.0003	0.0007	0.0005
$\nabla^2\rho(r)$	0.1567	0.4344	0.1566	0.4344	0.0002	0.0003	0.0002
$\|\lambda1\|/\|\lambda3\|$	0.1729	0.2525	0.1728	0.2525	0.1000	0.1286	0.1143
Distances						3.752	3.881

Note: #Parameters in a.u., Distances in Å

Table S5. Frontier Molecular Orbitals, HOMO and LUMO, Gap Values and Chemical Potential (μ), Electronegativity (χ), Global Hardness (η), Global Softness (S) and Global Electrophilicity Index (ω) Descriptors for Monomer and Dimers of ABT in Gas Phase and Water Solution by Using B3LYP/6-311++G Calculations**

B3LYP/6-311++G** Method								
Orbital	MONOMER		DIMER 1		DIMER 2			
	Gas	Water	Gas	Water	Gas	Water		
HOMO	-6.8137	-6.8246	-6.4573	-6.6260	-6.4246	-6.5688		
LUMO	-1.6245	-1.6300	-1.8286	-1.7443	-1.8313	-1.7524		
|GAP|	5.1892	5.1947	4.6287	4.8817	4.5933	4.8164		
DESCRIPTORS (eV)								
χ	4.2191	4.2273	4.1430	4.1852	4.1280	4.1606		
μ	-4.2191	-4.2273	-4.1430	-4.1852	-4.1280	-4.1606		
η	2.5946	2.5973	2.3144	2.4409	2.2967	2.4082		
S	0.1927	0.1925	0.2160	0.2048	0.2177	0.2076		
ω	3.4304	3.4401	3.7082	3.5880	3.7097	3.5941		
Orbital	DD2[b]		Adamantadine[c]	Chloroquine[d]			Oseltamivir[e]	
				S(-) Form	R(+) Form			
	Gas	Water	Water	Water	Water			
HOMO	-6.3457	-6.3892	-6.4736	-6.0055	-5.9865	-6.7375	-6.9906	
LUMO	-2.1279	-2.1633	-0.4218	-1.7061	-1.6844	-1.4558	-1.6245	
|GAP|	4.2178	4.2259	4.1116	4.2994	4.3021	5.2817	5.3661	
DESCRIPTORS (eV)								
χ	-2.1089	-2.1130	-2.0558	-2.1497	-2.1511	-2.6409	-2.6830	
μ	-4.2368	-4.2763	-3.3130	-3.8558	-3.8354	-4.0967	-4.3075	
η	2.1089	2.1130	2.0558	2.1497	2.1511	2.6409	2.6830	
S	0.2371	0.2366	0.2432	1.0748	1.0755	1.3204	1.3415	
ω	4.2559	4.3272	2.6695	3.4581	3.4194	3.1775	3.4578	

Note: [a]This work, [b]Karrouchi et al., 2023 for the C2 conformer of 5-((*1H*-benzo[d][1,2,3]triazol-1-yl)methyl)quinolin-8-ol (DD2) (Karrouchi et al., 2023), [c] Brandán, (2021), [d] Romano et al., (2020), [e]Vakili et al., (2021).

Note: $\chi = -[E(LUMO) - E(HOMO)]/2$; $\mu = [E(LUMO) + E(HOMO)]/2$; $\eta = [E(LUMO) - E(HOMO)]/2$; $S = \frac{1}{2}\eta$; $\omega = \mu^2/2\eta$